Journal of Alloys and Compounds 505 (2010) 685–691

Contents lists available at ScienceDirect

Journal of Alloys and Compounds

journal homepage: www.elsevier.com/locate/jallcom

# Growth characteristics and mechanism of carbides precipitated in WC–Fe composite coatings by laser induction hybrid rapid cladding

Shengfeng Zhou [a,*], Xiaoyan Zeng [b]

[a] School of Material Science and Engineering, Nanchang Hangkong University, Nanchang, Jiangxi 330063, PR China
[b] Wuhan National Laboratory for Optoelectronics, School of Optoelectronics Science and Engineering, Huazhong University of Science and Technology, Wuhan, Hubei 430074, PR China

ARTICLE INFO

*Article history:*
Received 6 August 2009
Accepted 18 June 2010
Available online 1 July 2010

*Keywords:*
Laser induction hybrid rapid cladding (LIHRC)
WC–Fe composite coating
Growth characteristics
Carbides

ABSTRACT

WC-reinforced Fe matrix composite coatings were prepared by laser induction hybrid rapid cladding (LIHRC). X-ray diffraction (XRD) was used to identify the phases and the growth characteristics of the precipitated carbides were observed by environmental scanning electron microscope (ESEM). The results show that WC particles are almost dissolved completely and interact with Fe-based alloy liquid in the molten pool to precipitate $M_6C$ carbides with different shapes during LIHRC. With increasing the weight percent of WC particles, the transition from the fine $M_6C$ carbides, which are precipitated in an intergranular network of the coarse α-Fe, to the coarse herringbone $M_6C$ eutectics and the primary faceted dendritic $M_6C$ occur and the partially dissolved WC particles with an alloyed reaction layer can be occasionally found in the composite coating. Moreover, the eutectic $M_6C$ carbides in herringbone shape grow in terms of the intergrowth mode of layer and slice, while the primary faceted dendritic $M_6C$ in equiaxial branched shape are only precipitated in the crossed region of the coarse eutectic carbides and grow in terms of dissolution and propagation.



## 1. Introduction

The ceramic–metal composite coatings with high hardness and high wear resistance are produced on the steel substrates of the low cost, which not only can exert the plasticity and toughness of the substrates, but also can make the best use of the high hardness and high wear resistance of the ceramic–metal composite coatings. As a result, the comprehensive properties of the substrate such as the combination of the high strength, high toughness, high hardness and high wear resistance may be improved markedly. Therefore, the techniques preparing the ceramic–metal composite coatings have a wide application potential in the fields of the surface repairing of the key components and the three-dimensional rapid manufacturing [1,2].

Now, the techniques preparing the ceramic–metal composite coating mainly include plasma spraying, arc welding, laser cladding and so on. Despite the introduction of high velocity oxy-fuel (HVOF) spraying, the obtained composite coatings have low to moderate adhesion to the substrate and still show porosity and cracking formation [3]. The arc welding technique has a very high efficiency, the metallurgical bonding between the composite coating and the substrates can be also generated [4]. However, the composite coatings have a high dilution and the substrates are susceptible to distortion due to the excessive energy input during the arc welding. The ceramic–metal composite coatings, which are prepared by laser cladding, not only have the properties of high wear and corrosion resistance, but also have the minimal dilution and the dense microstructure [5]. Additionally, both the bonding metals and the ceramic particles can be selected widely. For instance, the bonding metals may be Ni-based alloy, Co-based alloy and Fe-based alloy, the reinforcement phases may be the carbides, oxides or intermetallic such as WC, SiC, $ZrO_2$, $Al_2O_3$, $MoSi_2$ and NiAl. Therefore, the technique of laser cladding ceramic–metal composite coating has been received a continuous and extensive attention in recent years [6,7].

To improve the wetting properties between the ceramic particle and the bonding metal, WC particle with high hardness, certain plasticity and a good wettability by the molten metals is widely chosen as the reinforcement phase to manufacture metal-based ceramic composite components exposed to high wear intensities, as cutting tools or mining machinery. Many studies have investigated the microstructure and properties of Ni-based or Co-based WC composite coatings by laser cladding [8,9] showing that, the formation of coarse brittle phases, such as chromium borides and carbides, is largely responsible for cracking of the composite coatings. As a result, the common problems such as low cladding efficiency and the cracking susceptibility limit the application of laser cladding technique in reality.

* Corresponding author. Tel.: +86 791 3863026.
*E-mail address:* zhousf1228@163.com (S. Zhou).

0925-8388/$ – see front matter © 2010 Elsevier B.V. All rights reserved.
doi:10.1016/j.jallcom.2010.06.115

**Table 1**
The chemical composition of the bonding metal Fe-based alloy (wt.%).

| C | Si | B | Cr | Mn | Ni | Fe |
|---|---|---|---|---|---|---|
| 0.4–0.6 | 1.0–2.0 | 2.0–3.0 | 1.0–2.5 | 0.65 | 4.30 | Bal. |

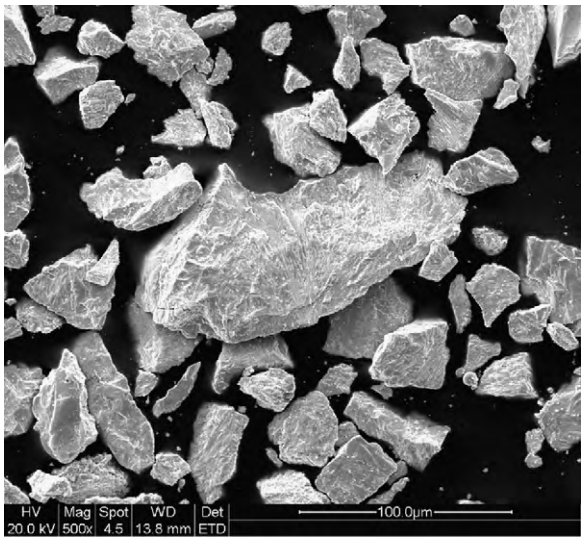


**Fig. 1.** Morphology characteristics of the cast WC particles.

In our previous work [10,11], laser induction hybrid rapid cladding (LIHRC) has been proposed as a new technique to increase the cladding efficiency and eliminate the cracks of cladding layer, the microstructure characteristics and crack-free reasons of Ni-based WC composite coatings by LIHRC were investigated in detail. However, so far no attempt has been made to deposit WC–Fe composite coatings by LIHRC. The objective of this paper is to investigate the use of LIHRC for preparing WC–Fe composite coatings and analyze the growth characteristics and mechanism of carbides precipitated in WC–Fe composite coatings.

## 2. Experimental procedures

In this experiment, A3 mild steel with a dimension of 110 mm × 45 mm × 7 mm was used as the substrate. Fe-based alloy powder, whose chemical composition was given in Table 1, was used as the bonding metal in size of 40–80 μm. The cast WC particles with a mean size of about 38 μm were used as the ceramic phase, whose chemical composition was the mixtures of WC + $W_2C$ eutectic and polygonal morphology is shown in Fig. 1. Prior to LIHRC, Fe-based alloy powder and the cast WC particles were homogeneously mixed to prepare the composite powders, in which the weight per cent of the cast WC particles was 20%, 35% and 50%, respectively.

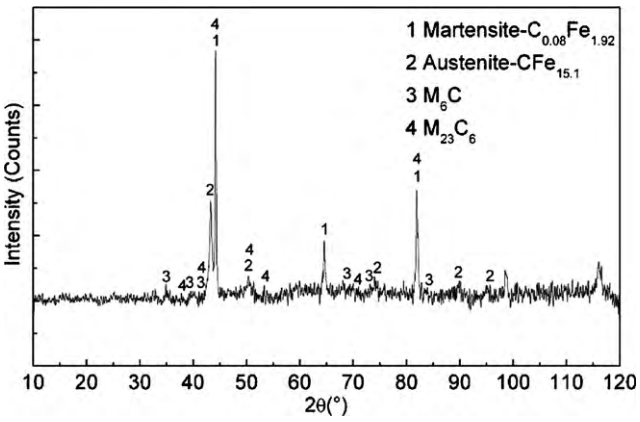


**Fig. 3.** X-ray diffraction results of Fe + 20 wt.% WC composite coatings by LIHRC.

The setup of LIHRC has been shown in Ref. [10]. The experiments of LIHRC were carried out using a Rofin-TR050 5 kW continuous wave $CO_2$ laser. The laser power was set at 5 kW, and the laser scanning speed was set at 600 mm $min^{-1}$. The beam spot was adjusted into the elliptical spot with an optical adjustment device. The major and minor axis of laser beam was 7 mm and 5 mm, respectively. The major axis was parallel to the direction of laser scanning speed. The operation frequency of induction heater was set at 30 kHz. The preheated average temperature of the substrate by LIHRC was set at 1123 K by adjusting the power of the induction heater. The powder feeder was the HUST-VI off-axial auto-feeding powder device. A shielding of Ar gas was used to blow the composite powder into the molten pool. The powder feeding rate was varied at 20–35 g/min. The powder nozzle was set at an angle of 35° with respect to the surface normal of the substrate, whose distance to the substrate was set at 10 mm.

After LIHRC, all the samples were cut, polished and etched by a solution of 10 vol. % $HNO_3$ + $C_2H_5OH$. Microstructure of WC–Fe composite coatings by LIHRC was examined under a Quanta 200 environmental scanning electron microscope (ESEM). The chemical composition of WC–Fe composite coatings was measured by energy dispersive spectrometry (EDS). X'Pert Pro X-ray diffraction (XRD) was used to analyze the phases (target: Cu, 40 kV, 40 mA).

## 3. Results and discussion

### 3.1. Microstructure of WC–Fe composite coating

For the composite coating containing 20 wt.% WC particles, the microstructure of WC–Fe composite coating prepared by LIHRC is shown in Fig. 2. It can be seen that a planar growth with a thickness of 10 μm and relatively coarse columnar dendrites are found at the coating-substrate interface. The result of the XRD analysis (Fig. 3) indicates that the composite coating is composed of marten-

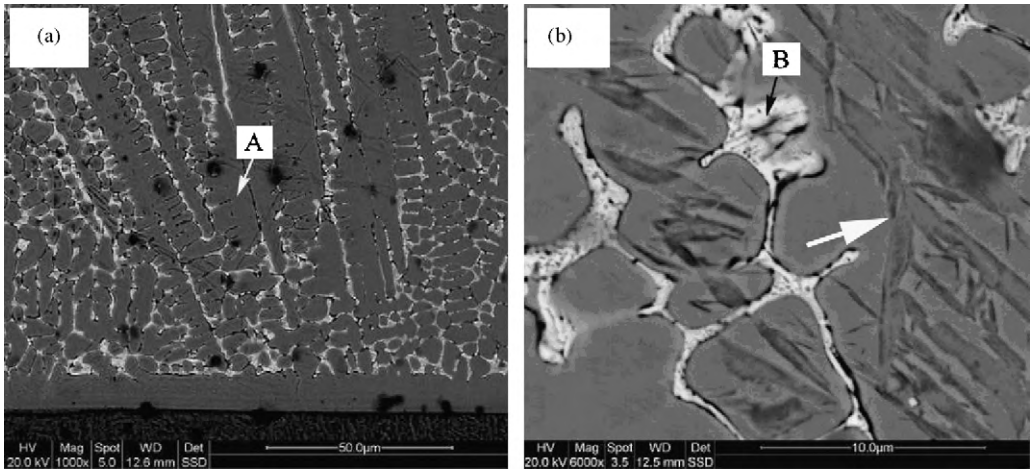


**Fig. 2.** Microstructure of Fe + 20 wt.% WC composite coating prepared by LIHRC: (a) at the interface of coating-substrate, (b) magnified micrograph of (a).

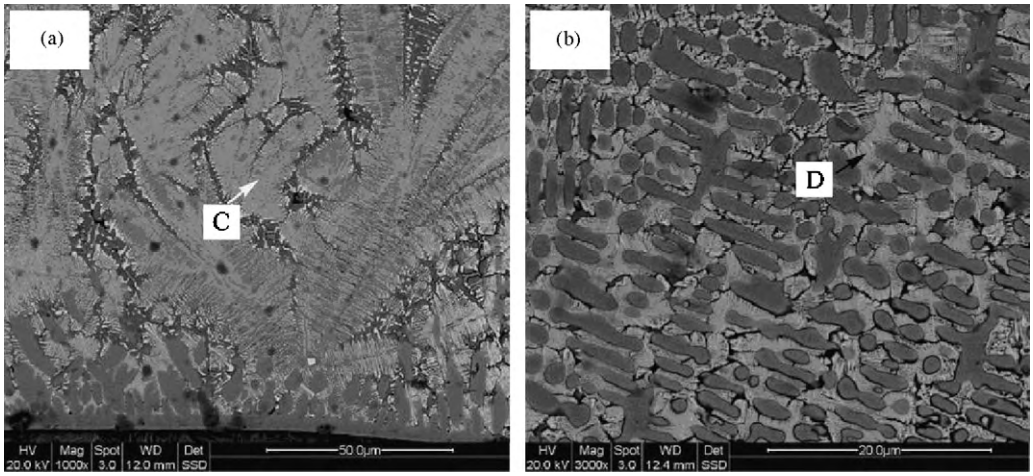


**Fig. 4.** Microstructure of Fe + 35 wt.% WC composite coating prepared by LIHRC: (a) at the interface of coating-substrate, (b) in the center of coating.

site (i.e. α-Fe corresponding to $C_{0.08}Fe_{1.92}$ composition), retained-γ (i.e. $CFe_{15.1}$), $M_6C$ and $M_{23}C_6$, and martensite with a tetragonal crystal structure is the prominent phase. The results of EDS analysis (Table 2) reveal that the dendrites (marked A in Fig. 2a) contain a high concentration of Fe, relatively small amounts of W and C, showing that the dendrites are the typical supersaturated solid solutions and transform into the acicular martensite (marked with white arrow in Fig. 2b) during LIHRC due to possible solid-state transformation. Combining the analysis of XRD (Fig. 3) and EDS (Table 2), it can be also seen from Fig. 2 that the fine $M_6C$ eutectics (marked B in Fig. 2b) approximately corresponding to $Fe_4W_2C$ composition are precipitated in an intergranular network of the coarse primary dendrites (i.e. the acicular martensite) which are enriched with tungsten content below 20 wt.%.

When the weight percent of WC particles increases to 35 wt.% in the composite coating, the microstructure of WC–Fe composite coating prepared by LIHRC is shown in Fig. 4. It can be also seen that a planar growth with a thickness of 5 μm and relatively small columnar dendrites, which are identified as the martensite by XRD analysis (Fig. 5), are observed at the coating-substrate interface. Combining the analysis of XRD (Fig. 5) and EDS (Table 2), it can be concluded that the coarse eutectics (marked C in Fig. 4a) are identified as the herringbone $M_6C$ (M = W, Fe, Ni, Cr) carbides containing about 65 wt.% tungsten content in the composite coatings. The previous studies [12,13] have also shown that the herringbone carbides, whose dendrite branches were evaluated to be at least 60 wt.% W, were known to belong to the $M_6C$ type.

When the weight percent of WC particles further increases to 50 wt.% in the composite coating, the microstructure of WC–Fe composite coating prepared by LIHRC is shown in Fig. 6. It can be seen that the bonding metal also has a planar growth but the thickness of the planar growth is only 2–3 μm, and relatively smaller columnar dendrites are also formed. Moreover, not only the herringbone eutectic carbides are precipitated in the composite coating, but also the dendritic carbides are precipitated in the center of the composite coating. The result of the XRD analysis (Fig. 7) indicates the existence of martensite, retained-austenite, $M_6C$, $W_2C$ and $M_7C_3$ in the composite coating. Based on EDS analysis (Table 2), it is evident that the average tungsten content in the areas of herringbone eutectic (marked E in Fig. 6a) is lower than that in herringbone dendrite branches (i.e. mentioned above at least 60 wt.%), while the dendritic carbides (marked F in Fig. 6b) contain a relatively large amount of W (67.33 wt.%).

According to the above results, the growth characteristics of Fe matrix can be deduced in the following. During LIHRC, the morphology of Fe matrix is determined by the solidification conditions such as the temperature gradient $G$ and the solidification rate $R$. At the bottom of the molten pool, the temperature gradient $G$ is relatively high but the solidification speed $R$ is very low, so that a planar growth is induced by the high ratio $G/R$. With increasing distance from the surface of substrate, the temperature gradient $G$ decreases gradually, while the solidification speed $R$ increases gradually, resulting in the decreasing of the ratio $G/R$. Therefore, a constitutional supercooling is soon generated and the planar solid/liquid interface becomes unstable, which induces the onset of a Fe-rich dendrite. With the process of solidification, carbon atoms from Fe-based alloy and the dissolution of WC particles which are driven by the concentration gradient can diffuse into the Fe-rich dendrite to form the supersaturated solid solution. Subsequently, the martensitic transformation is induced by the high cooling rate of LIHRC to form the acicular or the hidden acicular martensite with

**Table 2**
The chemical composition analysis of the marked location in Fig. 1.

| Location | Composition (wt.%) | | | | | |
|---|---|---|---|---|---|---|
| | C | Cr | Mn | Fe | Ni | W |
| A | 4.75 | 1.35 | 0.63 | 74.01 | 3.19 | 16.07 |
| B | 3.42 | 1.12 | 0.60 | 33.26 | 1.20 | 60.4 |
| C | 3.20 | 0.96 | 0.58 | 28.35 | 1.23 | 65.68 |
| D | 3.71 | 1.10 | 0.61 | 30.27 | 1.31 | 62.99 |
| E | 4.58 | 1.2 | 0.56 | 42.81 | 3.2 | 48.21 |
| F | 5.14 | 1.1 | 0.62 | 25.6 | 1.37 | 67.33 |

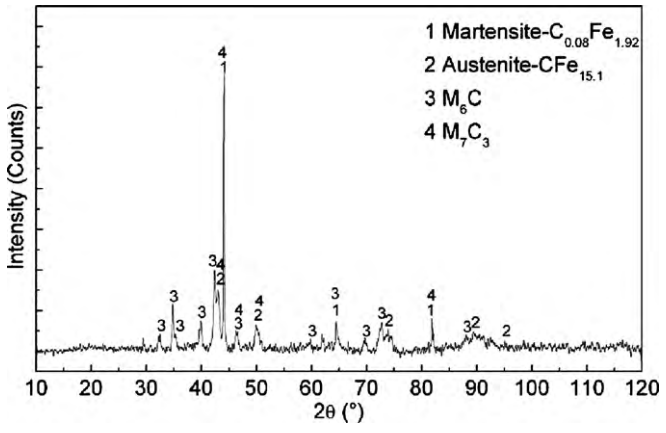


**Fig. 5.** X-ray diffraction results of Fe + 35 wt.% WC composite coatings by LIHRC.

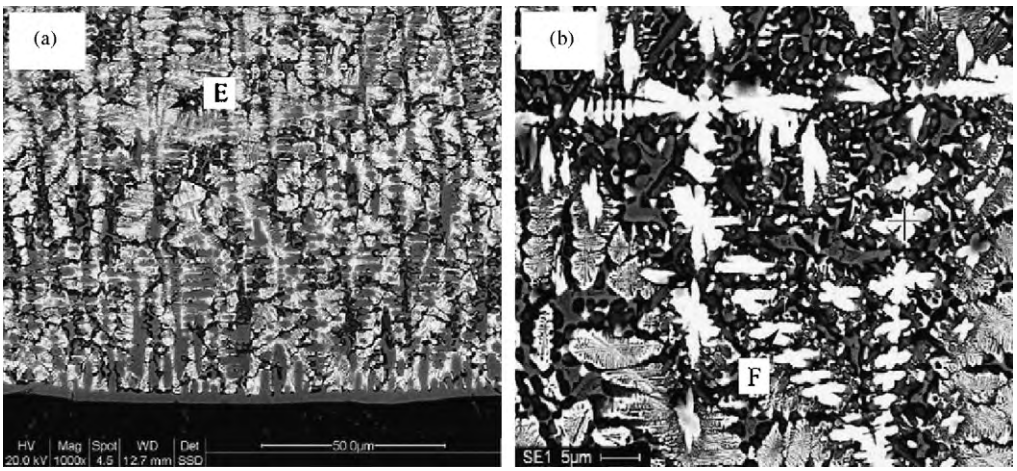


**Fig. 6.** Microstructure of Fe + 50 wt.% WC composite coating prepared by LIHRC: (a) at the interface of coating-substrate, (b) in the center of coating.

high W content (Figs. 2, 4 and 6). This is because a high concentration of W can be usually dissolved into α-Fe, while hardly dissolved in γ-Fe according to Fe–W–C phase diagram [14].

Moreover, due to the complete dissolution of WC particles during LIHRC, the herringbone eutectic carbides and the facet dendritic carbides are precipitated in the composite coating. The growth characteristics of the precipitated carbides will be discussed in detail as follows.

### 3.2. Growth characteristics of eutectic carbides

It can be found from the above results that the cast WC particles are almost dissolved completely, and the carbides with different morphology are precipitated in WC–Fe composite coatings. According to the Fe–W–C ternary phase diagram as shown in Fig. 8, the complicated reaction can take place in the molten pool during LIHRC as follows:

$$1973\,K: \quad L + WC + W \rightarrow M_6C \tag{1}$$

$$1773\,K: \quad L + W \rightarrow M_6C + Fe_3W_2 \tag{2}$$

$$1653\,K: \quad L + Fe_3W_2 \rightarrow M_6C + \alpha \tag{3}$$

$$1608\,K: \quad L + \alpha \rightarrow \gamma + M_6C \tag{4}$$

Moreover, the W atoms diffusing into Fe-based alloy liquid are increased due to increasing the weight percent of WC particles. When the temperature of the molten pool approaches the above temperature range as listed in reactions (1)–(4), the hypoeutectic reaction can take place, resulting in the precipitation of the eutectic carbides during the rapid solidification. As a result, the deficient W region in front of the solid/liquid interface can induce WC particles to dissolve continually. Obviously, increasing the weight percent of WC particles reduces the amount of primary α-Fe phase and increases the volume fraction of the eutectic carbides. The dissolution process of WC particles is that WC particles react with the Fe-based alloy liquid, and then are gradually dissolved to precipitate the eutectic carbides, which have two distinct characteristics as follows:

(1) With increasing the weight percent of WC particles, the carbides go through a transition of the fine $M_6C$ eutectic precipitated in an intergranular network of the coarse α-Fe to the coarse $M_6C$ eutectic precipitated in the composite coating (Figs. 2, 4 and 6).
(2) The coarse $M_6C$ eutectic carbides which have the coarse dendritic branch present a growth characteristic of the herringbone shape. The gray microstructure of BSE micrograph as shown in Fig. 9 is Fe-based interdendrite matrix phase. The result of EDS analysis show that the gray microstructure contains 4.28% C, 1.18% Cr, 54.33% Fe, 2.68% Ni and 37.53% W (wt.%), showing that the gray microstructure is in rich Fe and W in relatively larger amounts to form a typical supersaturated solid solution. That is because W atoms in large amounts diffuse into the iron-

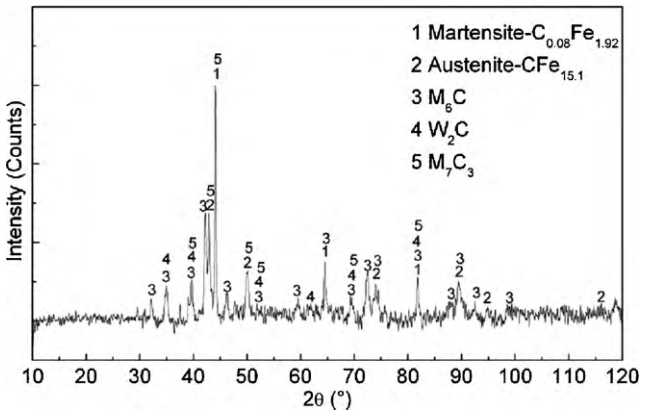


**Fig. 7.** X-ray diffraction results of Fe + 50 wt.% WC composite coatings by LIHRC.

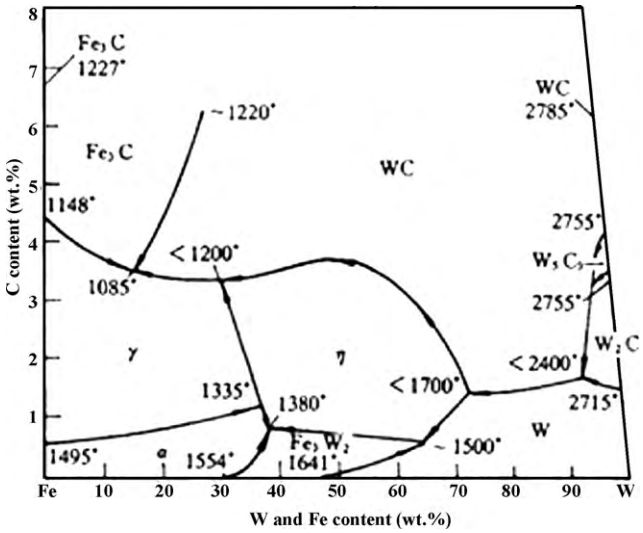


**Fig. 8.** Liquidus projection of the Fe–W–C ternary phase diagram.

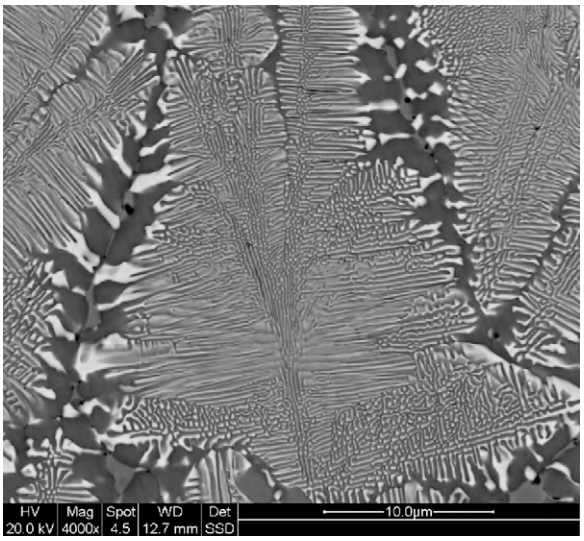


**Fig. 9.** Backscattered electron image of eutectic carbides in Fe + 35 wt.% WC composite coating.

based phase (i.e. α-Fe) during the precipitation process of $M_6C$ eutectic carbides. The similar microstructure characteristics of functionally graded tungsten carbide coatings on M2 high speed tool steel by laser cladding were also found by Fishman et al. [15]. Moreover, according to the analysis reported in Ref. [16], the herringbone $M_6C$ eutectic carbides can grow in terms of the intergrowth mode of layer and slice, whose trunk grows parallel to the temperature gradient and branch grows perpendicular to the temperature gradient. Therefore, the growth process of the herringbone eutectic carbides can be explained in the following.

Firstly, the above reaction can take place, resulting in precipitating the carbides, which grow into the dendrites at the initial stage of the rapid solidification due to constitutional supercooling (CS). After that, the carbides grow rapidly to form the coarse dendritic branch and the W atoms diffuse into the liquid iron, the supersaturated iron-based phase containing rich W atoms as the subsequent phase can grow on the surface of the primary carbides. Consequently, the double phase nucleation sites with the interface of the intergrowth are formed, and then supply the atoms for the neighboring phase to grow harmoniously, which depends on the diffusivity of the solute atoms, such as Fe, W and C, to diffuse continually on the interface of the carbides and the iron-based phase. Furthermore, the eutectic two phases are characterized by the non-facet growth of the unshaped interface, so that the eutectics are formed by the intergrowth of the primary carbide and the iron-based phase, both of which present the different crystal structures (Fig. 9). Therefore, the herringbone $M_6C$ eutectic carbides grew in terms of the intergrowth mode of layer and slice during LIHRC.

Additionally, when the weight percent of WC particles increase to 50%, $M_6C$ eutectic carbides grow perpendicular to the coating-substrate interface at the bottom of the molten pool. However, the growth direction of the eutectic carbides is disordered in the center of the composite coating as shown in Fig. 10a, which can be explained by the following reasons. The violent stirring and convection are induced by thermocapillarity in the molten pool [17], resulting in the non-uniform distribution of the solutes and the temperature in front of solid/liquid interface due to the longer lifespan in the center of the molten pool compared to that at the bottom of the molten pool. Therefore, the disordered eutectic morphology is observed in the center of the composite coating.

Notice that the facet dendritic carbides are precipitated in the crossed region of the eutectic carbides (marked G in Fig. 10a), and the partially dissolved coarse WC particles (marked H in Fig. 10a) whose amount fraction in the sum of the primary WC particles is less than 5% interact with Fe-based alloy to form the alloyed reaction layer with a thickness of 1–3 μm (Fig. 10b). As a result, the changes of the local concentration are brought about due to the formation of W and C enriched regions around the coarse WC particles during their partial dissolution. The growth of the herringbone eutectic carbides which contain about 62% W is formed in the area surrounding the partially dissolved WC particle (Fig. 10b). Concerning the facet dendritic carbides, their growth characteristics are discussed in detail in the following.

### 3.3. Growth characteristics of the facet dendritic carbides

The microstructure is characterized by the presence of the primary faceted carbide dendrites as shown in Fig. 10a and magnified in Fig. 6b, whose tungsten content is about 67 wt.% (Table 2) when the weight percent of WC particles increases to 50 wt.%, as can be expected that the primary carbides are precipitated on the tungsten-rich side in the hypereutectic range of the phase diagram (Fig. 8). The value seems to be in good agreement with that of 65 wt.% W detected in the herringbone eutectic carbides by EDS analysis. Obviously, the faceted dendrites and the herringbone eutectics should belong to two forms of $M_6C$ carbide, whose morphology is determined by the carbide growing either as a primary phase or as a eutectic constituent. Moreover, the

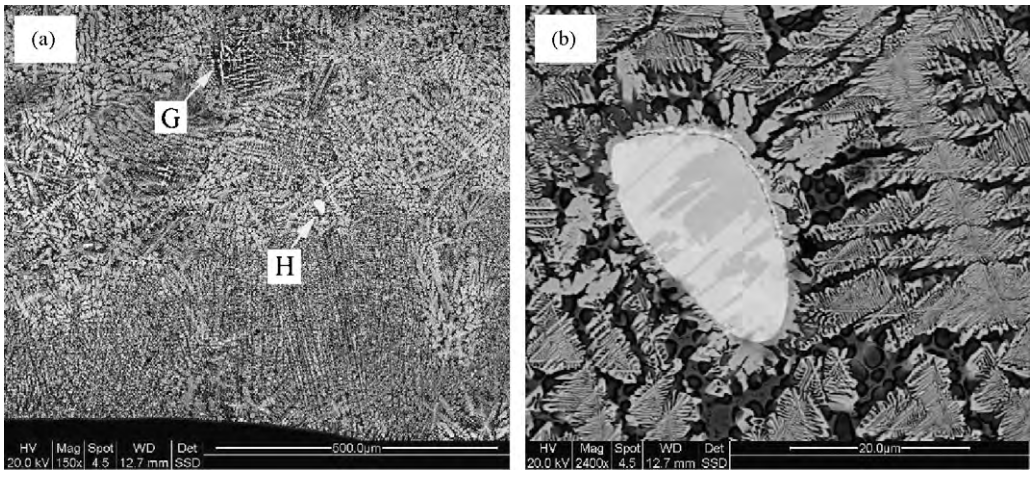


**Fig. 10.** Characteristics of interface in Fe + 50 wt.% WC composite coating by LIHRC: (a) the interface of coating-substrate, (b) the interface of WC particle and Fe matrix.

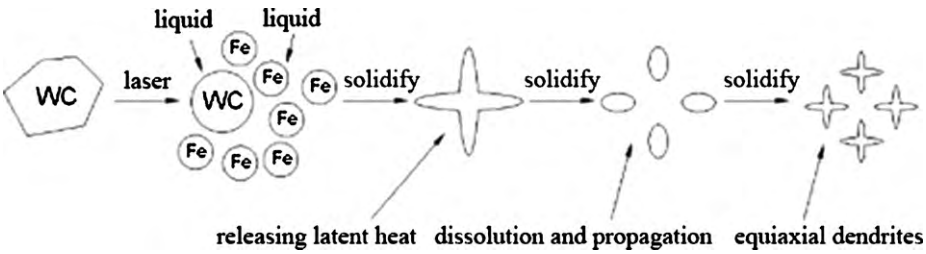


**Fig. 11.** Dissolution process of WC particles and precipitation process of carbides.

faceted dendritic carbides have also two characteristics as follows.

(1) The primary faceted $M_6C$ dendrites are precipitated around the partially dissolved WC particles and grow into an equiaxial branched shape; (2) the primary faceted $M_6C$ dendrites in equiaxial shape, which locate in the center of the composite coating as shown in Fig. 10a, are only precipitated in the crossed region of the coarse eutectic carbides, indicating that the equiaxial $M_6C$ dendrites are precipitated prior to the coarse eutectic carbides. It can be explained by the following reasons.

That is because the incompletely dissolved WC particles can provide the preferential heterogeneous nucleation sites for $M_6C$ carbides. However, these $M_6C$ carbides cannot grow into the facet dendritic carbides until their nucleation size exceeds the critical size of the heterogeneous nucleation. At the top of the composite coating, the nucleation size of fewer $M_6C$ carbides may exceed the critical size to grow into the dendritic structure due to higher temperature and lower supercooling of the molten pool. Therefore, fewer incompletely dissolved WC particles can supply the heterogeneous nucleation for $M_6C$ carbides. Nevertheless, with increasing distance from the surface to the center of the molten pool, both the amount of the incompletely dissolved WC particles and the supercooling of the molten pool are increased gradually. As a result, the nucleation size of many $M_6C$ carbides can exceed the critical size and they continue to grow up so that the liquid side forms a W-rich concentration region in front of the solid/liquid interface. Moreover, the convection and the stirring are often relatively more violent in those regions, such as the center of the molten pool and the crossed region of the eutectic carbides, compared to that in the other regions of the molten pool. Consequently, the front of the solid/liquid interface is surrounded by the supercooled liquid and continually suffers from the impact of the temperature fluctuation and the concentration fluctuation, so that the latent heat has a difficulty in releasing to the surrounding liquid during the growth of the dendritic carbides. The temperature is increased by the released latent heat at the root of the dendritic arm, which contains 6.64 C, 2.68 Cr, 67.46 Fe, 2.2 Ni and 21.02 W (wt.%) by EDS analysis. It is obvious that the root of the dendritic arm contains a relatively larger amount Fe, relatively smaller amount W compared to the carbides enriched with tungsten (Table 2). Therefore, the root of dendritic arm enriched Fe with lower melting point is susceptible to be dissolved by the released latent heat so that it is separated into several pieces, which independently grow into a new dendrite to finish the propagation of the dendritic carbide with further decreasing the temperature gradient as shown in Fig. 11. Furthermore, due to the rapid solidification of LIHRC, the dendrites formed by the mentioned above propagation have no enough time to grow up, the released latent heat also have no enough energy to dissolve all the dendrites, so that the dendrites are usually precipitated and grow into the fine and equiaxial $M_6C$ carbides in the crossed region of the coarse eutectic carbides as shown in Figs. 6b and 10a. Chen et al. [18] also reported the similar growth morphology of TiC carbide in laser cladding TiC/FeAl composite coating. To sum up, the primary faceted dendritic $M_6C$ carbides in equiaxial branched shape are precipitated in the crossed region of the coarse eutectic carbides and grow in terms of the mode of dissolution and propagation.

## 4. Conclusions

(1) With increasing distance from the surface of substrate, a planar growth, column dendrites are formed and Fe matrix are transformed into the martensite enriched with W and retained-austenite (approximately $CFe_{15.1}$ composition) during laser induction hybrid rapid cladding. Moreover, WC particles are almost dissolved completely and react with Fe-based alloy liquid in the molten pool to precipitate the eutectic and facet dendritic $M_6C$ carbides during the rapid solidification.

(2) With increasing the weight percent of WC particles, the partially dissolved coarse WC particles are occasionally observed in the composite coating and react with Fe-based alloy liquid to form an alloyed reaction layer around WC particle, and the carbides go through a transition of the fine $M_6C$ eutectics precipitated in an intergranular network of the coarse $\alpha$-Fe to the coarse herringbone $M_6C$ eutectics and the primary facet $M_6C$ dendrites precipitated in the composite coating. Moreover, the eutectic $M_6C$ carbides in herringbone shape grow in terms of intergrowth mode of layer and slice, while the primary faceted dendritic $M_6C$ carbides are only precipitated in the crossed region of the coarse eutectic carbides and grow in terms of dissolution and propagation.

## Acknowledgements

The supports of this work by the Aviation Science Foundation of China (grant No. 2009ZE56013), Jiangxi Province Education Department Foundation of China (grant No. GJJ10507) and the doctoral start-up fund research of Nanchang Hangkong University (grant No. EA200901170) are gratefully acknowledged.

## References

[1] Y.T. Pei, V. Ocelik, T.Th.M. De Hosson, Acta Mater. 50 (2002) 2035.
[2] M. Zhong, W. Liu, G. Ning, L. Yang, Y. Chen, J. Mater. Process. Technol. 147 (2004) 167.
[3] R.S. Lima, B.R. Marple, J. Ther. Spray Technol. 16 (2007) 40.
[4] M. Suban, J. Tusek, J. Mater. Process. Technol. 119 (2001) 185.
[5] J.A. Vreeling, V. Ocelik, J.Th.M. De Hosson, Acta Mater. 50 (2002) 4913.
[6] R. Ananadkumar, A. Almeida, R. Colaco, R. Vilar, V. OCelik, J.Th.M. De Hosson, Surf. Coat. Technol. 201 (2007) 9497.
[7] S. Yu, Y. Liu, L. Ren, W. Li, Metall. Mater. Trans. A 37 (2006) 3639.
[8] M. Duraiselvam, R. Galun, V. Wesling, B.L. Mordike, J. Laser Appl. 18 (2006) 297.
[9] C.P. Paul, H. Alemohammad, E. Toyserkani, A. Khajepour, S. Corbin, Mater. Sci. Eng. A 464 (2007) 170.
[10] S. Zhou, Y. Huang, X. Zeng, Q. Hu, Mater. Sci. Eng. A 480 (2008) 564.
[11] S. Zhou, Y. Huang, X. Zeng, Appl. Surf. Sci. 254 (2008) 3110.

[12] H. Brandis, E. Haberling, H.H. Weigland, in: M.H.Q. Wells, L.W. Lhebrier (Eds.), Processing and Properties of High Speed Tool Steels, Met. Soc. AIME, 1980, p. 1.
[13] M. Boccalini Jr., A.V.O. Correa, H. Goldenstein, Mater. Sci. Technol. 15 (1999) 621.
[14] Pierre Villars, H. Alan Prince, Okamoto, Handbook of Ternary Alloy Phase Diagram, ASM International, 1995, p. 108.
[15] M.R. Fishman, E. Rabkin, P. Levin, N. Frage, M.P. Dariel, A. Weisheit, R. Galun, B.L. Mordike, Mater. Sci. Eng. A 302 (2001) 106.
[16] P. Hassen, Physical Metallurgy, Cambridge Univ. Press, 1978, p. 126.
[17] P.A. Carvalho, R. Vilar, Surf. Coat. Technol. 91 (1997) 158.
[18] Y. Chen, H.M. Wang, Mater. Lett. 57 (2003) 1233.